

Simultaneous ground-satellite observations of meso-scale auroral arc undulations

T. Motoba,¹ K. Hosokawa,² Y. Ogawa,¹ N. Sato,¹ A. Kadokura,¹ S. E. Milan,³ and M. Lester³

Received 24 October 2011; revised 12 April 2012; accepted 27 April 2012; published 9 June 2012.

[1] We present simultaneous ground-based and in situ measurements of a train of meso-scale (about 100–300 km) auroral arc undulations, occurring in the postmidnight sector (~ 1 MLT) between 0040 UT and 0054 UT on September 21, 2009. The undulations appeared at the auroral poleward boundary, and then moved eastward with a speed of 0.9–2.2 km s⁻¹. Dynamic behaviors of the associated meso-scale ionospheric plasma flows and current systems were also detected with the ground-based magnetometer and radar measurements within the all-sky camera field-of-view. During the interval of interest, simultaneous Cluster observations in the central near tail region (11–14 R_E down tail) were available, and especially the ionospheric footprint of Cluster 2 (CL2) was close to the optical auroral forms. CL2 observed strong fluctuations in the in situ magnetic field with amplitude of 5–10 nT whenever a bright arc area, and its trailing adjacent area, of the auroral undulations passed its ionospheric footprint. Such in situ magnetic field changes at CL2 could be considered as a manifestation of localized upward and downward field-aligned current sheets moving eastward at the central near-Earth tail boundary, linked to the meso-scale auroral undulation structures.

Citation: Motoba, T., K. Hosokawa, Y. Ogawa, N. Sato, A. Kadokura, S. E. Milan, and M. Lester (2012), Simultaneous ground-satellite observations of meso-scale auroral arc undulations, *J. Geophys. Res.*, *117*, A06213, doi:10.1029/2011JA017291.

1. Introduction

[2] A series of large-scale bright auroral undulations with wavelengths of 400–1000 km is frequently seen in the post-midnight to early morning sector during substorm recovery phase. The auroral undulations have widely been known as “omega bands” [e.g., Akasofu and Kimball, 1964; Akasofu, 1974; Opgenoorth *et al.*, 1983]. Omega bands have a characteristic structure which consists of bright tongues interleaved with dark regions and propagate eastward at a velocity in the range of 0.4–2.0 km s⁻¹. Most of the drifting omega bands are accompanied by magnetic pulsations with periods of 5–40 min and amplitudes from 10 nT to more than 500 nT. Such pulsations are observed with magnetometers on the ground as Ps6 pulsations [e.g., Saito, 1978], which are more predominant in the east-west (D) component. In electrodynamics of omega bands in the ionosphere, it has been considered that successive bright and dark

regions correspond to pairs of localized upward and downward field-aligned currents (FACs) moving eastward [e.g., Wild *et al.*, 2000], and that Ps6 pulsations on the ground are generated by the passage of the resulting ionospheric Hall currents above the observing points. However, it has still been unclear where and how the omega band-related FACs are generated in the magnetotail. Some previous numerical simulation studies predicted that the omega band formation and the related FAC generation are driven by some kind of instability in the magnetotail equatorial plane, such as Kelvin-Helmholtz instability [Janhunen and Huuskonen, 1993] and electrostatic interchange instability [Yamamoto *et al.*, 1997].

[3] Although the auroral omega bands in the ionosphere have frequently been observed for decades after the pioneer paper by Akasofu and Kimball [1964], there have been few observations of their counterparts in the magnetosphere. Jorgensen *et al.* [1999] presented a case in which Ps6 pulsations were observed simultaneously on the ground and in the magnetospheric equatorial plane around geosynchronous orbit. Their results suggested that the magnetospheric counterpart of omega bands/Ps6 pulsations originates from a localized region in the near-Earth magnetotail. A recent study by Wild *et al.* [2011] compared the ground-based all-sky imager measurements of omega bands with the in situ field and plasma measurements from the conjugate region in the near-Earth magnetotail. Although they did not find a clear one-to-one correspondence between variations in the

¹National Institute of Polar Research, Tokyo, Japan.

²Department of Communication Engineering and Informatics, University of Electro-Communications, Tokyo, Japan.

³Department of Physics and Astronomy, University of Leicester, Leicester, UK.

Corresponding author: T. Motoba, National Institute of Polar Research, 10-3 Midori-cho, Tachikawa, Tokyo 190-8518, Japan. (motoba.tetsuo@nipr.ac.jp)

©2012. American Geophysical Union. All Rights Reserved.

ionosphere and magnetosphere, they suggested that that Alfvén waves in the plasma sheet $\sim 8 R_E$ tailward of the Earth are responsible for the generation of FACs that cause omega bands/Ps6 pulsations observed on the ground. However, none of the previous in situ observations has confirmed how the magnetospheric counterpart develops longitudinally with eastward drifting auroral forms in the ionosphere.

[4] In this study, we present a case study providing direct magnetosphere-ionosphere linkage for the meso-scale (about 100–300 km) auroral undulations seen at the poleward edge of the post-midnight aurora, on the basis of the simultaneous ground-satellite observations. The undulations, which were observed with the ground-based all-sky camera (ASC) at Tjörnes (TJO, 66.20°N, 17.12°W, geomagnetic latitude: 66.40°N, MLT: \sim UT) in Iceland, occurred in the late stage of the 21 September 2009 substorm event reported by Motoba *et al.* [2010, 2011]. The meso-scale ionospheric structures behind the auroral undulations described here were also observed with ground-based magnetometer and radar measurements in Iceland. We found that the ionospheric structures were in many respects similar to those of the classical auroral omega bands summarized above, except for their scale size. During this particular event, the Cluster spacecraft was located near the southern lobe boundary–plasma sheet ~ 11 – $14 R_E$ down tail, and especially the ionospheric footprint of Cluster 2 (CL2) was close to the observed auroral structures. The CL2 location was favorable for detecting the near tail FAC signatures associated with the auroral arc undulations by using the Cluster Fluxgate Magnetometer (FGM) instrument. In this study, the energetic electron data taken with the Cluster Plasma Electron And Current Experiment (PEACE) instrument were used to discriminate the near-Earth tail regions that have different plasma regimes. In order to link the FAC signatures at CL2 with the eastward drifting auroral undulations, we also discuss the near-Earth tail FAC features, especially from the viewpoints of electromagnetic energy and longitudinal motion, by combining in situ observations at Cluster 1 which was separated $\sim 2 R_E$ dawnward of CL2.

2. Observations

2.1. Ground-Based Optical, Magnetometer and Radar Observations

[5] Figure 1 presents an overview of the auroral arc undulation event observed by the ground-based ASC and magnetometer at TJO. The ASC is a white light all-sky CCD camera operating at a standard video rate (30 Hz). Each image used in this study is taken with an exposure time of ~ 1.07 s (32 video frames). Figure 1a shows a time series of the H component of the magnetic field at TJO for the interval from 0000 UT to 0100 UT on September 21, 2009. The vertical dashed line indicates the onset time (0024 UT) of a weak substorm, defined by the start of magnetic negative bay developing with the auroral activation (for details, see Motoba *et al.* [2010]). In this study, we focus on the late stage of the weak substorm activity, especially the time interval from 0040 UT to 0054 UT shaded with gray in Figure 1a. Figures 1b and 1c respectively show a keogram (magnetic north-south direction) and an ewogram (magnetic east-west direction) obtained from the ASC images at TJO for the 14 min interval from 0040 UT to 0054 UT. A

fundamental limitation of ground-based optical observations is the ambiguity in determining the location of an optical feature without any knowledge of the altitude profile of the emission intensity. In this study, we assume that the altitude of the main optical emission is 110 km. This assumption means that the observed optical features were mainly produced by precipitating electrons with characteristic energy of several keV [cf. Rees, 1963]. Moreover, it is deduced that such keV electrons result from a field-aligned acceleration of lower-energy (≤ 1 keV) electrons of PSBL origin. As evident in these panels, some meso-scale auroral structures drifted eastward along the poleward boundary of diffuse aurora, which consisted of weak optical pulsations (~ 150 km southward of zenith). The latitudinal and longitudinal scales of each structure were roughly 50–100 km and 100–300 km, respectively. Figure 1d presents the H (black), D (red), and Z (blue) components of the magnetic field at TJO for the same interval as Figures 1b and 1c. During this interval, a characteristic quasiperiodic magnetic field oscillation with a period of ~ 2 min and amplitude of 10–30 nT was observed. As seen in Figure 1a, such a magnetic field oscillation occurred under condition of a fairly stable, weak westward electrojet (negative bay), with values of -100 nT to -150 nT and extensive coverage to the Scandinavian sector (not shown). The vertical dashed lines indicate the timings of the marked positive peaks in the quasiperiodic magnetic D component variation: (i) 0044:00 UT, (ii) 0045:30 UT, (iii) 0048:20 UT, (iv) 0050:10 UT, and (v) 0052:13 UT. The ASC images at these timings are presented in Figure 1e. At the times of (i) and (ii), the auroral arc elongating mostly in the east-west direction passed slightly equatorward of TJO, while the zenith of the ASC was covered by the dark area just poleward of the arc. In addition, each positive peak in D component lagged the minimum in Z component by a few tens of seconds. These features resembled the typical signatures of the previous omega bands/Ps6 seen in the ground-based optical and magnetometer data [cf. Opgenoorth *et al.*, 1983], although the period of the magnetic field oscillation was shorter than the typical Ps6 period range. Also at the other three peaks (iii, iv and v), the other auroral arcs passing across TJO were seen, but they were developing into vortex-like or spiral-like forms. The eastward propagation speeds estimated from ewogram were about 2.2 km s^{-1} for the first three auroral arcs (i–iii) and about 0.9 km s^{-1} for the other arcs (iv–v). Both propagation speeds were in the range of typical omega band speeds.

[6] We also used the coherent high-frequency (HF: 8–20 MHz) radar at Bykkvibaer (63.77°N, 20.54°W) in southwestern Iceland, which is the Iceland East radar of the international Super Dual Auroral Radar Network (SuperDARN) [Chisham *et al.*, 2007], to observe ionospheric electric fields (plasma flows) in the vicinity of the optical auroral forms. This radar has a field-of-view (FOV) that extends northeastward, which covers almost entire FOV of the ASC at TJO. During the interval of interest, this radar was operating with a special camping mode providing higher temporal and spatial resolution measurements of the ionospheric electric field within the FOV of the ASC at TJO [see Hosokawa *et al.*, 2010, and references therein] for details of this mode. In this mode the radar operated with 15 km range separations giving higher spatial resolution. In addition, six beams (beams 5–10) were scanned clockwise like 5, 7, 6, 7,

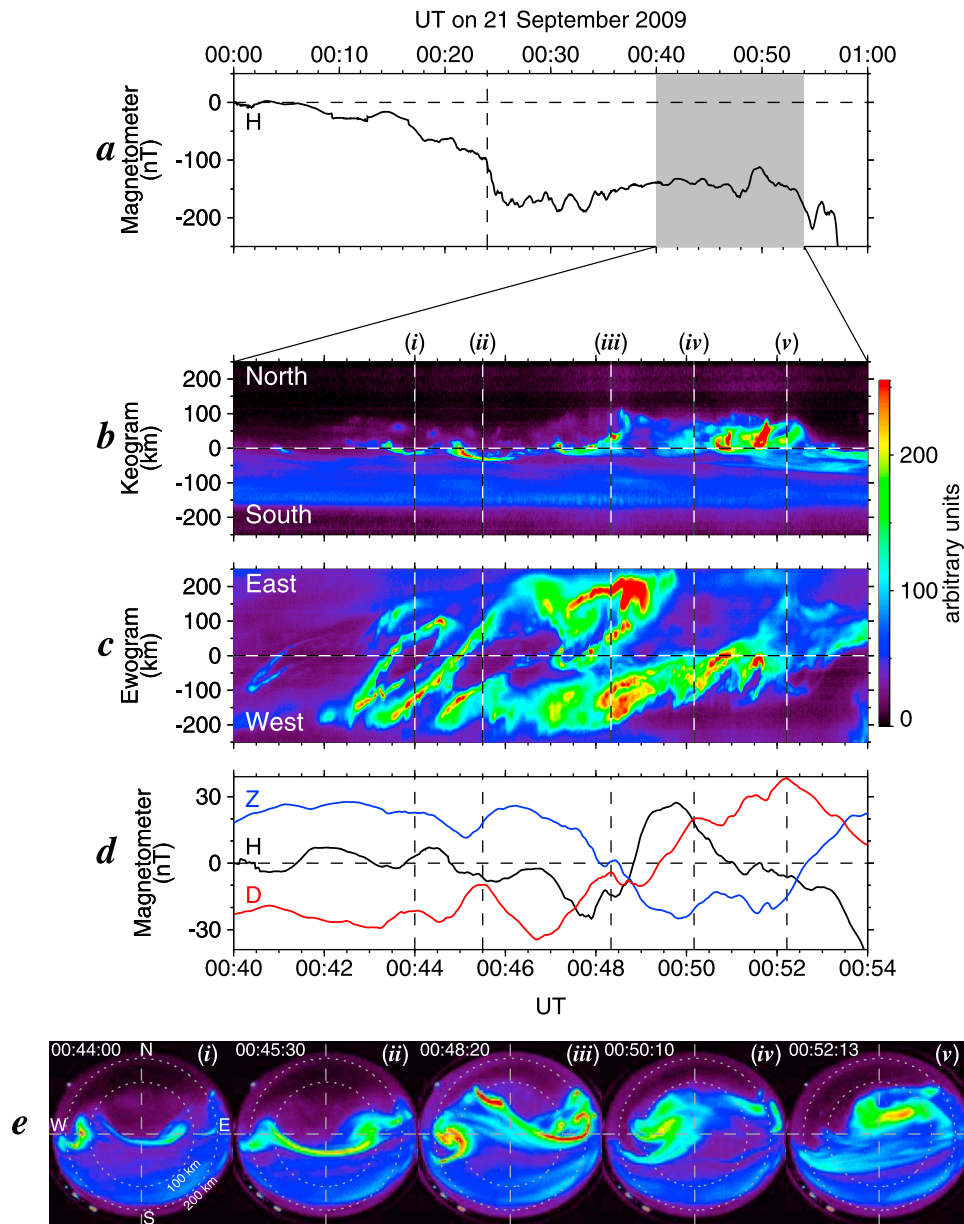


Figure 1. Ground-based optical and magnetometer measurements at TJO on September 21, 2009. (a) H component of the magnetic field for the interval of 0000 UT to 0100 UT. Keogram (b) north-south slices and (c) east-west slices of ASC images, and (d) three components (H: black, D: red, and Z: blue) of the magnetic field for the interval of 0040 UT to 0054 UT. (e) ASC images at the (i)–(v) times. The top, down, right, and left sides of each image are poleward, equatorward, eastward, and westward, respectively.

8, 7, 9, 7, 10, 7, with a dwell time of 2 s for each. As a result, we obtained the high-time resolution (4 s) line-of-sight (LOS) velocity data along beam 7 covering the zenith of ASC at TJO, as well as the two-dimensional LOS velocity data with a full scan every 20 s.

[7] Figures 2a and 2b respectively show keograms obtained by slicing ASC images along beam 7 and LOS Doppler velocities from beam 7 with a temporal resolution of 4 s. Both data are plotted as a function of range gate and time. Here, the ground range for the backscatter is determined from the slant range of each cell by assuming straight-line propagation to an altitude of 110 km [cf. Milan *et al.*,

2002]. This enabled us to examine the spatial relationship between the optical forms and the associated radar backscatters. Positive (negative) Doppler shifts correspond to velocities toward (away from) the radar, i.e., southeastward (northeastward). Figure 2c shows time series of the LOS velocity from beam 7, range gate 21 (closest to the zenith of the ASC at TJO), which is marked by horizontal dashed line in Figure 2b. Figure 2d shows the beam 7-aligned component of the equivalent currents (black curve) derived from the ground magnetometer data at TJO, together with the distribution of the two-dimensional equivalent current vectors (gray arrows) every 5 s. The up- and right-pointing

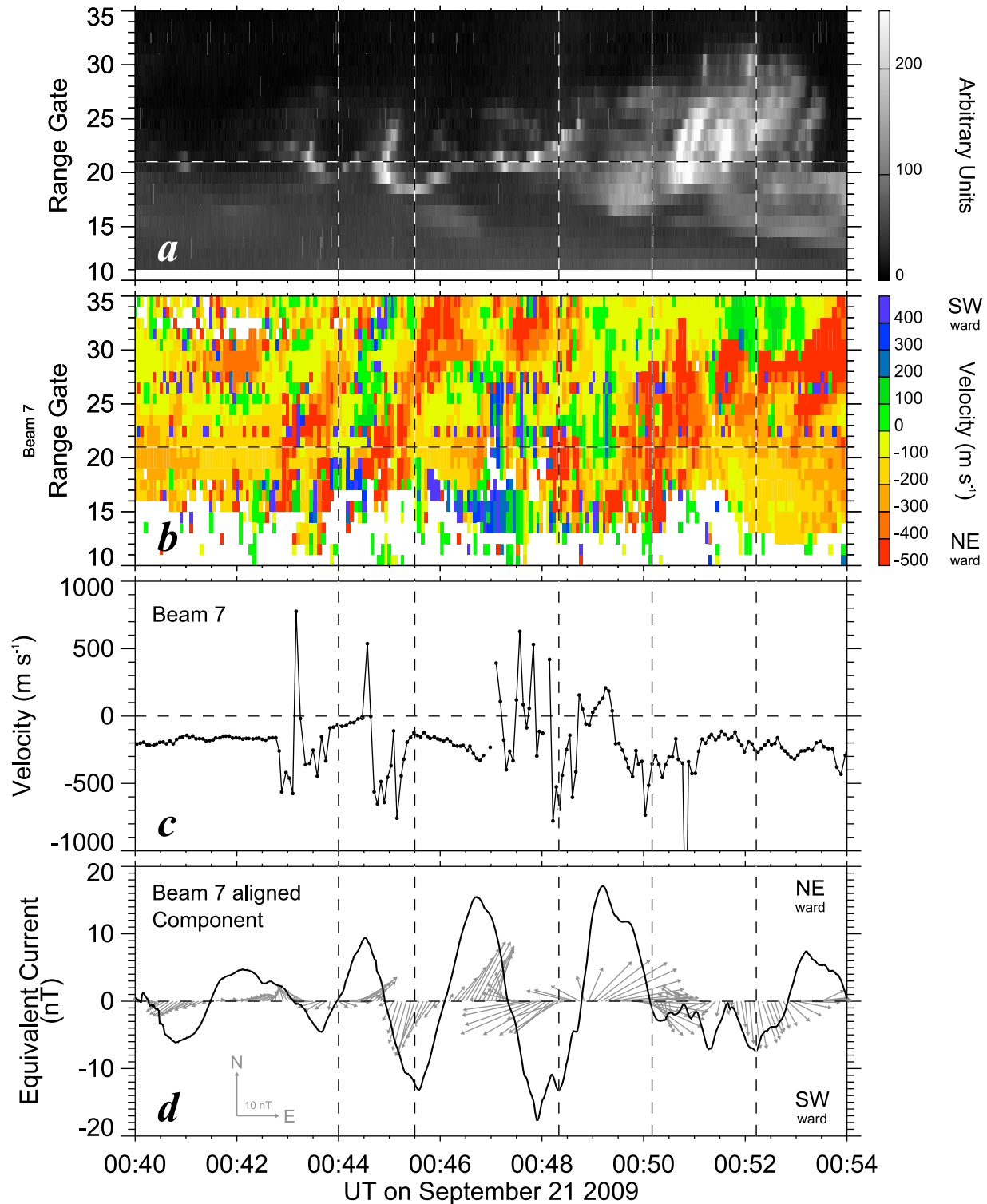


Figure 2. Comparison between the ground-based optical, radar, and magnetometer data for the interval of 0040 UT to 0054 UT. (a) Keogram along beam 7 of the Iceland East radar, plotted in the range-time format. (b) LOS Doppler velocities from beam 7. (c) LOS Doppler velocity at gate range 21, beam 7. (d) Distribution of equivalent current vectors (gray arrows) every 5 s and their beam 7-aligned component (black thick line) deduced from ground magnetometer at TJO. Vertical dashed lines are drawn at the same times as (i)–(v) in Figure 1.

vectors correspond to northward and eastward currents, respectively. To derive the equivalent current patterns, we have subtracted the 3 min running average from the horizontal magnetometer data. The beam 7-aligned component of the equivalent current vectors is estimated by using azimuthal angle ($\sim 41.0^\circ$ east of due north) of beam 7 at range gate 21. Positive value corresponds to a current flowing northeastward (i.e., opposite to the LOS of beam 7). Vertical dashed lines are the same as those in Figure 1. As seen in Figure 2b, the radar detected clear shared flows (pair of positive and negative LOS plasma flows) with a velocity of 200 km s^{-1} to 500 km s^{-1} or more around the first three auroral arcs (*i-iii*). Around the other arcs (*iv-v*) developing into the spiral-like or vortex-like forms, on the other hand, the sheared flows were unclear. Also in Figure 2c, pairs of the quasiperiodic flow deflections were evident around the first three auroral arcs (*i-iii*), although the background flow of about -200 km s^{-1} was superposed on them. The negative (i.e., northeastward) background flow appears to be related to the weak negative bay superposed on the quasiperiodic magnetic field oscillation as the background current system. In the case of a homogeneous conductivity distribution in the ionosphere, the plasma should flow in the opposite direction to the ionospheric equivalent current (i.e., Hall current). If such an ideal condition was fulfilled, the beam 7-aligned plasma flow (Figure 2c) and equivalent current (Figure 2d) would point in opposite directions (i.e., when plasma flow is northeastward (negative deflection), the equivalent current is southwestward (negative deflection), and vice versa). However, we find that both variations were not always matched for some of the time interval, in particular between 0045:30 UT and 0047:30 UT and after 0050:00 UT. The discrepancy would be due to steep conductivity gradients in the vicinity of the auroral arc undulations, leading to a more complicated relation between both variations.

[8] Figure 3 shows the two-dimensional distributions of the LOS velocity superposed on the ASC images at 0044:00 UT (*i*) of Figure 1e) and 0045:30 UT (*ii*) of Figure 1e). The regions of brighter aurora are outlined with white contours for detailed comparison. At 0044:00 UT, the LOS velocity in the eastern half of the radar FOV for this mode (beams 9–10) tended to be negative (positive) on the poleward (equatorward) side of the east-west aligned auroral arc. In contrast, the flow directions in the western half (i.e., the fainter arc or dark region) of the radar FOV (beams 5–8), where the arc was fainter, or even absent, were reversed, i.e., positive (negative) on the poleward (equatorward) side of the fainter arc. At 0045:30 UT, the east-west aligned auroral arc became more prominent slightly equatorward of the zenith. At this time, the radar detected negative (positive) LOS velocities on the poleward (equatorward) side of the arc. This pattern was very similar to that seen in the eastern half of the radar FOV (beams 9–10) at 0044:00 UT. In both cases, the plasma flow appears to diverge from the more intense arc, i.e., the LOS velocity is northeastward (southwestward) on the poleward (equatorward) side of the arc. This would imply that there exists an upward FAC.

[9] Figure 4 shows 16 ASC images ($\leq 75^\circ$ in zenith angle) taken every 15 s between 0041:45 UT and 0045:30 UT, together with the Cluster 2 (CL2) footprint (red square) calculated by the Tsyganenko 1996 (T96) model [Tsyganenko,

1995]. Each image is projected onto a geographic map of the Icelandic region at an assumed altitude of 110 km. The selected geomagnetic latitudes (every 2 degrees) and magnetic local times (MLT, every 30 min) in altitude adjusted corrected geomagnetic (AACGM) coordinates [Baker and Wing, 1989] are superposed on the images. The white and gray solid circles show the location of TJO and the distance of 150 km from TJO at 110 km altitude, respectively. During this interval, CL2 was located at $(X, Y, Z) = (-13.4, -1.8, -1.5 R_E)$ in GSM and the traced footprint was about 150 km or more westward away from TJO. At 0042:00 UT an initial bright auroral spot appeared around the poleward boundary of diffuse aurora (very close to the CL2 footprint), and then developed into a wave-like undulation. The other two arcs following the first one also underwent similar temporal evolution. They consisted of three individual auroral arc undulations (*i*, *ii*, and *iii*) and propagated eastward. Each numbered arc corresponds to that shown in Figure 1e. During this interval, we found that the bright east/west edges of the auroral arc undulations and the dark areas in between alternately passed through the CL2 footprint.

[10] In order to deduce spatial scale and propagation speed of the meso-scale auroral undulation structures in the near tail region, on the other hand, we projected the auroral images at 0043:30 UT, 0044:00 UT, and 0045:00 UT onto the Y-Z plane at the X position ($\sim 13.4 R_E$) of CL2, using the T96 model (Figure 5). The CL2 location in the Y-Z plane is shown by red square. From Figure 5, we found that the average spatial scales of the bright structures projected at the CL2 location were $0.5\sim 1.0 R_E$ in the Y direction and $1.0\sim 1.5 R_E$ in the Z direction, and that their thickness was a few thousand kilometers. In addition, the propagation speed of the auroral arcs (*i-iii*) with the speed of about 2.2 km s^{-1} in the ionosphere was found to be translated to $\sim 40 \text{ km s}^{-1}$ in the dawnward direction in the near-Earth tail.

2.2. Conjunction Observations Between ASC and Cluster

[11] Figure 6 shows the energetic electron and magnetic field observations between 0030 UT and 0054 UT, obtained from the PEACE [Johnstone et al., 1997] and FGM [Balogh et al., 2001] instruments onboard CL2. The PEACE experiment comprises two sensors, high- and low-energy electron analyzers (HEEA and LEEA), which cover a combined energy range 1 eV to 25 keV. The first to third panels present energy-time spectrograms of electron differential energy flux (DEF) in directions parallel, perpendicular, and anti-parallel to the local magnetic field, obtained from the spin resolution (~ 4 s) PEACE data. From the fourth to eighth panels, the total magnetic field strength ($|B|$), three components (B_x , B_y , and B_z in GSM coordinates), and magnetic inclination (defined by $\arctan(B_z/(B_x^2 + B_y^2)^{0.5})$) obtained from the full-resolution (~ 0.045 s) FGM data are presented. The vertical dashed line indicates the time (0045:05 UT) at which the average energy of the electrons at CL2 began to increase with decreasing $|B|$ and $|B_x|$. Before ~ 0040 UT, the magnetic field at CL2 was characterized by large negative B_x and nearly zero B_z . The energetic electron fluxes of all components were dominant in the range from 100 eV to 2 keV. The in situ field and particle observations indicate that CL2 for this interval was located in the highly stretched southern lobe region. From ~ 0040 UT

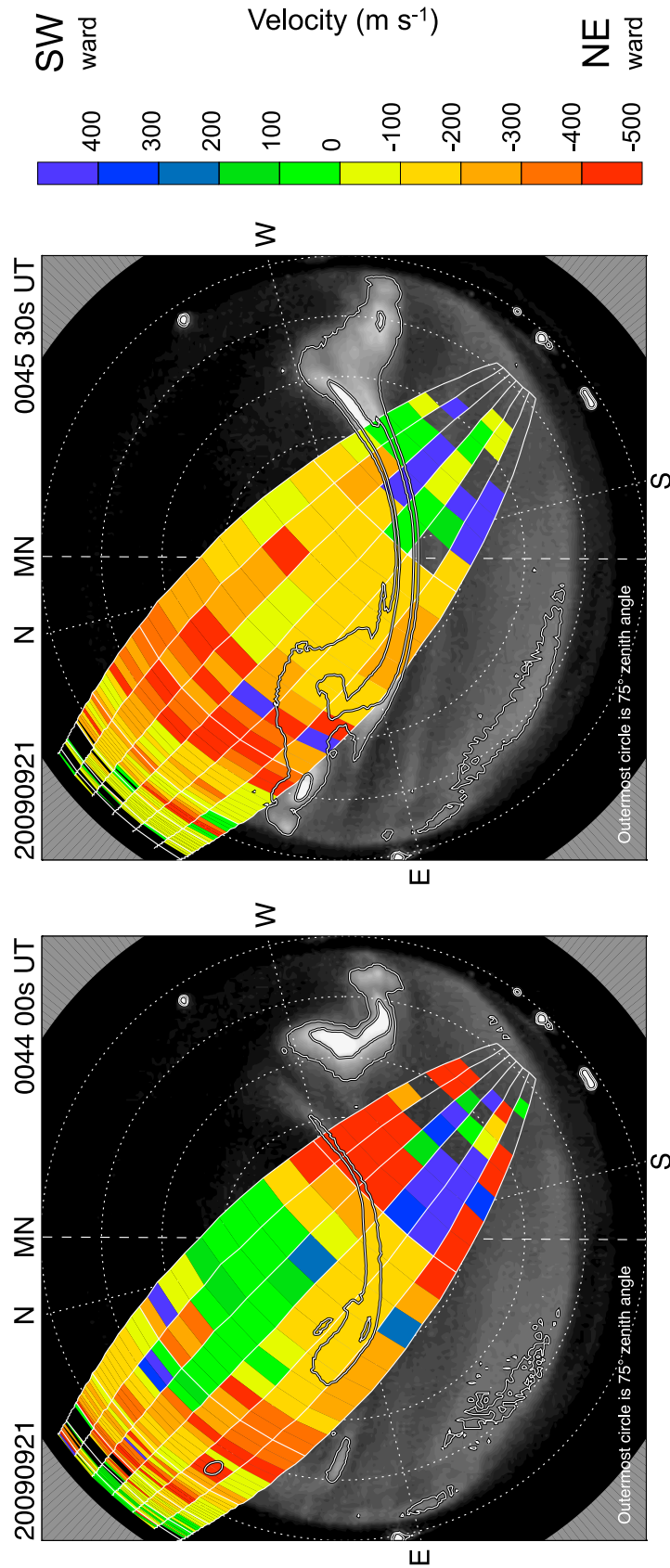


Figure 3. ASC images at the (i) and (ii) times of Figure 1e, with the LOS velocities from the Iceland East radar overlotted. The brighter auroral areas are outlined by white contours.

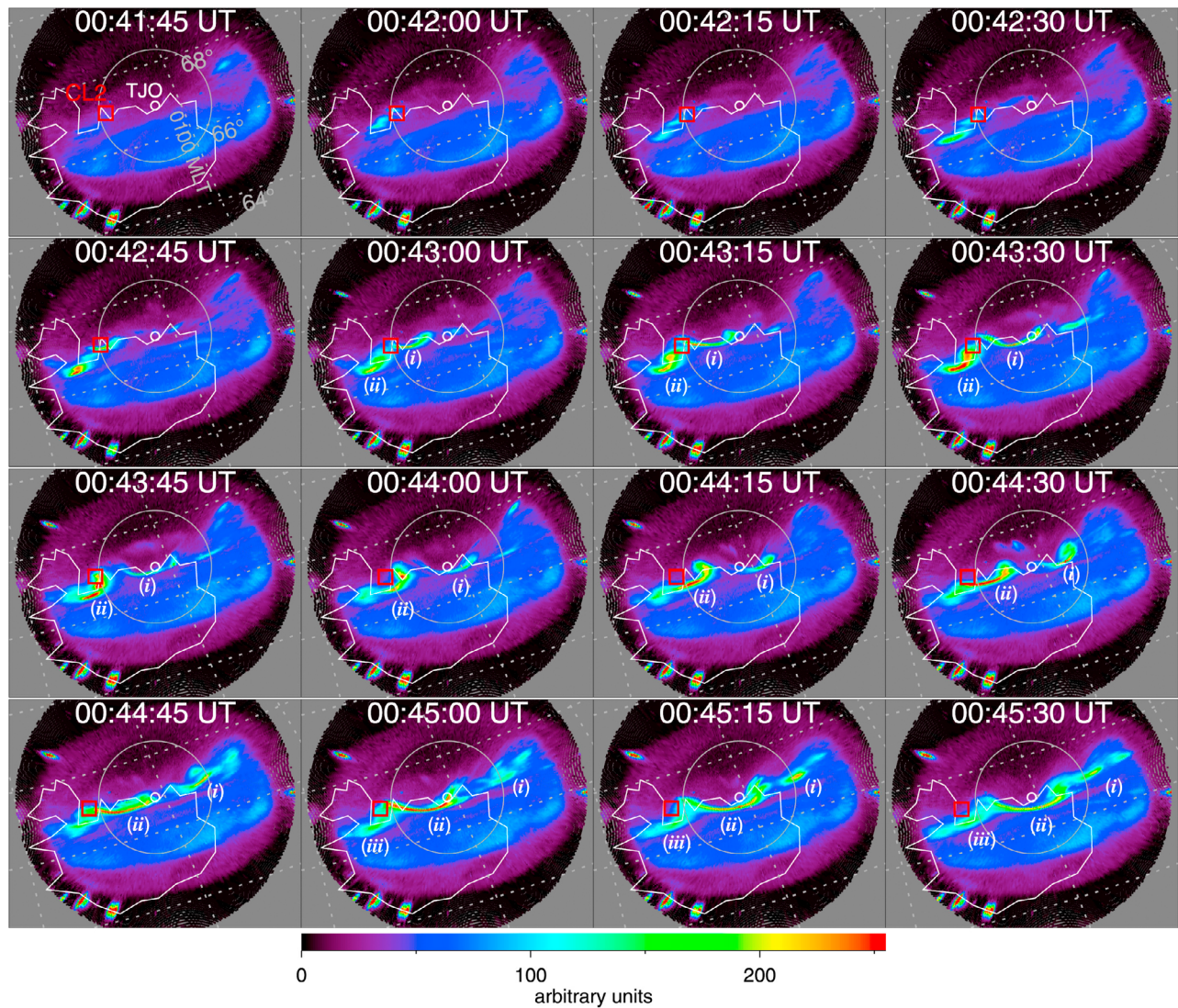


Figure 4. ASC images mapped on the geographic coordinate every 15 s for the interval of 0041:45 UT to 0045:30 UT. Red square denotes the CL2 footprint calculated from the T96 model. Dotted lines show geomagnetic latitudes and magnetic local times in AACGM coordinates.

to 0045:05 UT, the magnetic field and energetic electrons at CL2 showed different characteristics from those before \sim 0040 UT. Although B_x at CL2 still remained negative values in the range of -30 nT to -40 nT, large

fluctuations in the range of 0 nT to 15 nT were seen in B_z as well as B_y . The magnetic inclination slightly increased with fluctuations in the range of 0° to 20° . During the same interval, the average energy of the electrons was almost the

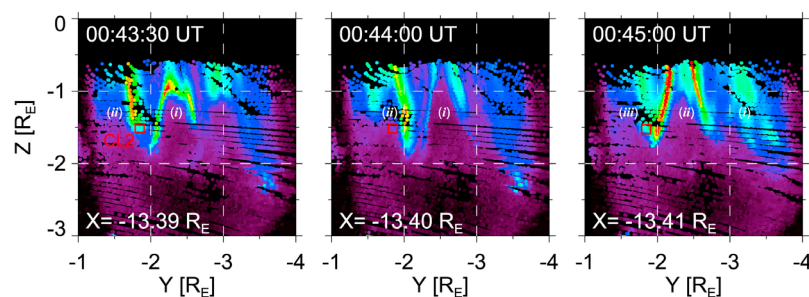


Figure 5. ASC images at 0043:30 UT, 0044:00 UT, and 0045:00 UT projected on the magnetotail Y-Z plane at the X position of CL2 using the T96 model. The view is from the magnetotail. Red square indicates the CL2 location.

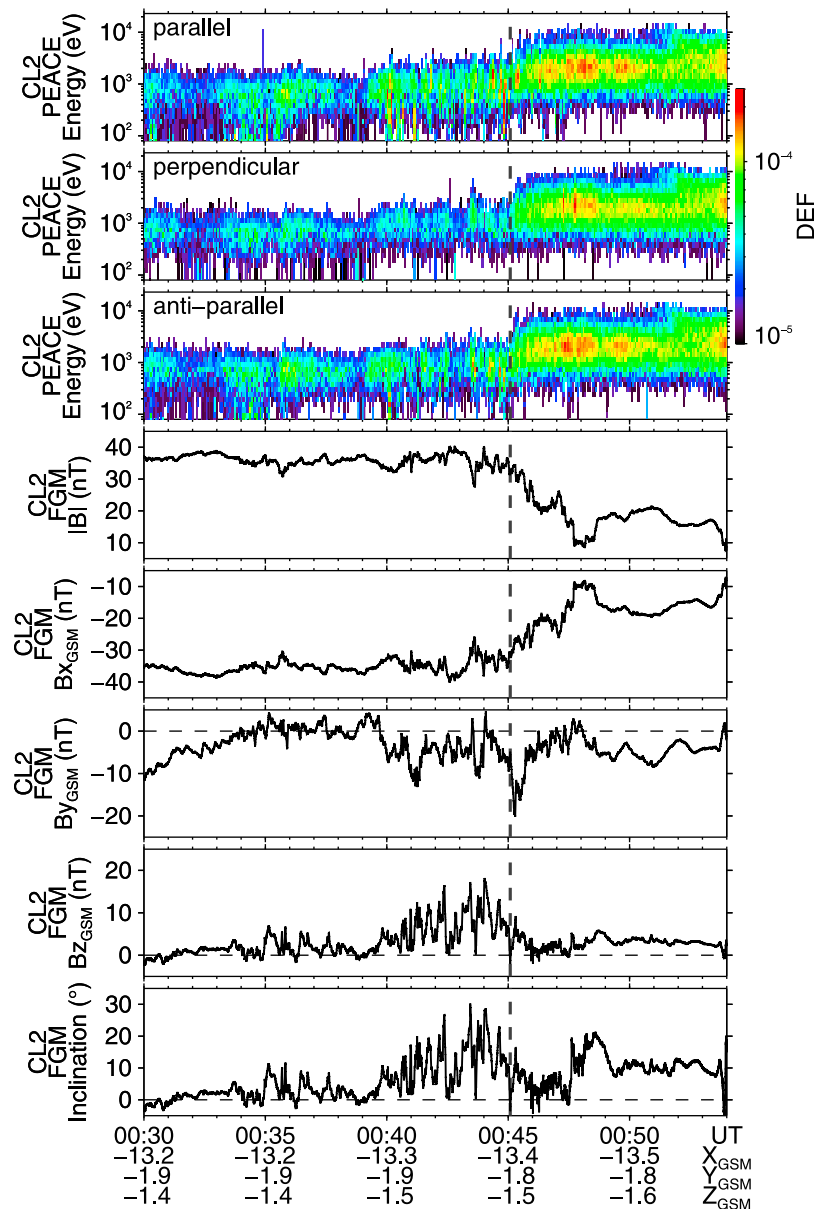


Figure 6. PEACE and FGM data given from CL2 for the interval of 0030 UT to 0054 UT on September 21, 2009. From top to bottom, energy-time spectrograms of electron differential energy flux in directions parallel, perpendicular, and anti-parallel to the local magnetic field, the total magnetic field ($|B|$), three components of the magnetic field in GSM coordinates, and magnetic inclination. Vertical dashed line indicates the timing when the average energy of the electrons at CL2 began to increase with decreasing $|B_x|$ (or $|B|$).

same as the previous one, but the fluxes of the field-aligned components were slightly enhanced. Both measurements suggest that during this interval CL2 was very close to the plasma sheet boundary layer (PSBL), probably in the intermediate region between the southern lobe and PSBL. After 0045:05 UT, $|B|$ and $|B_x|$ began to decrease steeply from ~ 35 nT to ~ 10 nT, while the peak value of B_z was relatively smaller than just before 0045:05 UT. Although the peak value of the magnetic inclination also decreased (less than 10°) just after 0045:05 UT, it increased again to 10° or more after 0048 UT. Just after 0045:05 UT, a large negative excursion was detected in B_y . The average energy of the

electrons began to increase from several hundred eV to a few keV with decreasing $|B|$ and $|B_x|$. Such dramatic field and particle changes at CL2 indicate that CL2 crossed the PSBL region. After 0047 UT the energetic electrons were characterized by the dense central plasma sheet (CPS) like population with the higher energy range of 1.0 keV to 10.0 keV. The crossing of CL2 from the southern lobe to PSBL and then the entering into CPS are more likely to be due to a dynamical change of the near-Earth tail topology (thickening of plasma sheet), because the movement of CL2 was insignificant during the short period. As shown in Figure 4, the ionospheric footprint of CL2 was very close to the auroral arc undulations

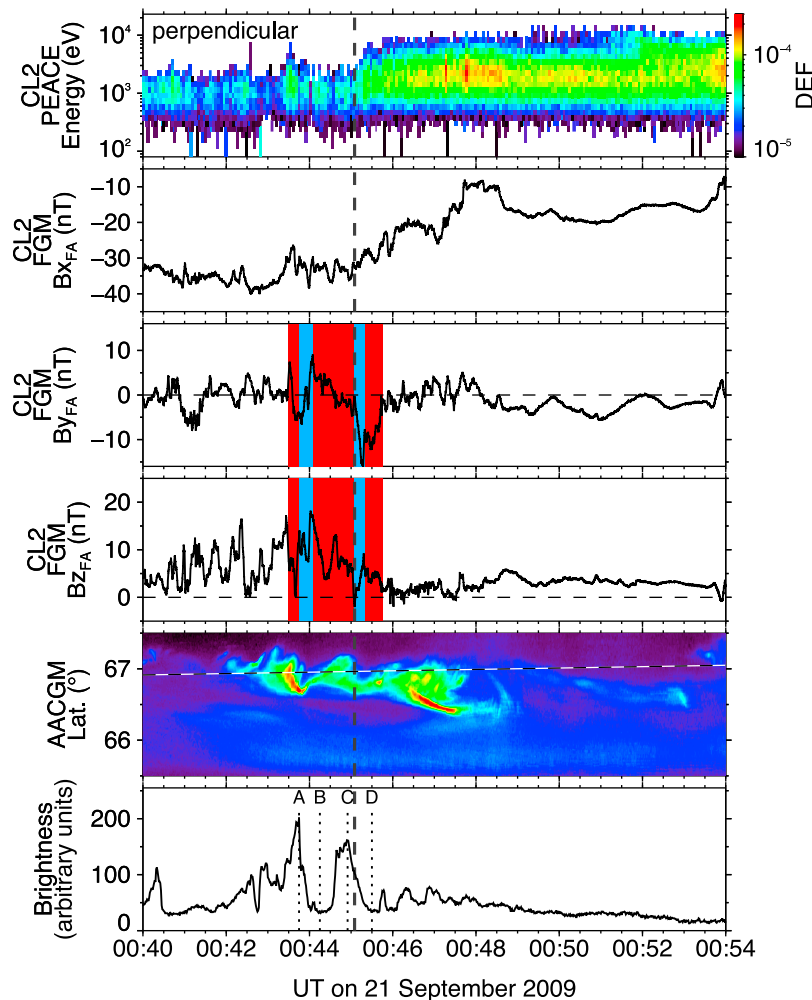


Figure 7. From first to fourth panels, perpendicular component of electron differential energy flux of the PEACE data at CL2, and three components of the FGM magnetometer data at CL2 (but shown in FA coordinates) for the interval of 0040 UT to 0054 UT. Fifth panel shows a keogram sliced along the magnetic meridian at the CL2 footprint, while sixth panel a time series of the auroral brightness just at the CL2 footprint. The dotted lines A and C (B and D) indicate the marked maxima (minima) in the auroral brightness. Vertical dashed line is the same as that in Figure 6. In the third and fourth panels, approximate local FAC signatures at CL2 deduced from our hypothesis are color-coded (red: upward FAC, blue: downward FAC). That is discussed in more detail in section 3.3.

(*i-iii*) exactly during the interval when CL2 crossed from the southern lobe to PSBL in the near-Earth tail.

[12] Figure 7 shows a more direct comparison between the in situ measurements at CL2 and the auroral features at its ionospheric footprint for the interval from 0040 UT to 0054 UT. The vertical dashed line is drawn at the same time (0045:05 UT) as that in Figure 6. The first panel of Figure 7 shows energy-time spectrograms of perpendicular DEF as reference. The second to fourth panels present the Bx, By, and Bz components of the magnetic field, which are transformed to a field-aligned (FA) coordinate system. In the FA coordinate system, the Z component is parallel to the Z axis in GSM coordinates and is positive northward. The X component is parallel to the projection of the average magnetic field between 0040 UT and 0045 UT on the X-Y plane in GSM coordinates and is positive earthward. The Y component is a right-handed orthogonal set ($Y = Z \times X$),

positive westward. The Y and/or Z components of the in situ magnetic field in FA coordinates help us to identify the FAC signatures in the near-Earth tail region [cf. *Ohtani et al.*, 1988] (to be discussed later). The fifth panel shows a keogram between 65.5° and 67.5° geomagnetic latitudes, sliced along the MLTs of the track of the CL2 footprint. The horizontal dashed line indicates the geomagnetic latitude of the CL2 footprint. The bottom panel shows time series of the auroral luminosity at the CL2 footprint, which is calculated by averaging over 3×3 pixels centered on the CL2 footprint estimated from the T96 model. From 0043 UT to 0046 UT, the auroral luminosity at the CL2 footprint indicated large fluctuations, consisting of local maxima at the timings (A and C) when the CL2 footprint encountered the bright eastward and westward edges of the (*ii*) auroral arc (see Figure 4), and local minima at the timings (B and D) when the CL2 footprint encountered the dark areas adjacent to the (*ii*) and (*iii*) arcs. In

analogy with the current systems in omega bands [e.g., *Wild et al.*, 2000], we expect that the bright (dark) area of the auroral arc undulations corresponds to the upward (downward) FAC region. During this interval, therefore, it is thought that the four FACs, upward (A)/downward (B)/upward (C)/downward (D), successively passed the CL2 footprint with the eastward drifting auroral structures. Interestingly, around the time when the successive local maxima and minima in the auroral luminosity were detected at the CL2 footprint, CL2 detected larger B_y and B_z field fluctuations.

[13] During this event, the other three Cluster satellites, Cluster 1 (CL1), Cluster 3 (CL3), and Cluster 4 (CL4), were also located in the near-Earth tail region, but separated from CL2 in the X and Y directions. Here we look into the differences and similarities among the spacecraft. CL1 was located at $(X, Y, Z) = (-12.2, -3.8, -1.9 R_E)$ in GSM: $\sim 1.0 R_E$ earthward and $\sim 2.0 R_E$ downward of CL2. On the other hand, both CL3 and CL4 were almost in the same region: CL3 was located at $(X, Y, Z) = (-11.6, -3.1, -1.9 R_E)$ in GSM, whereas CL4 at $(-11.7, -3.1, -2.0 R_E)$ in GSM). The location was separated by $\sim 2.0 R_E$ in the earthward direction and by $\sim 1.0 R_E$ in the dawnward direction from CL2. From first to seventh panels of Figure 8, energy-time spectrograms of electron DEF in directions perpendicular to the local magnetic field, magnetic field strength, and three components of the magnetic field in FA coordinates at CL1 (red), CL3 (green), and CL4 (blue) are presented for the interval of 0040–0054 UT. Similar to CL2, the three satellites also detected the PSBL crossing signatures, characterized by both a decrease in $|B_x|$ and an increase in the average energy of the electrons. However, the PSBL crossing times were different between spacecraft. CL3 and CL4 underwent the PSBL crossing at 0050:30 UT (shown by the first vertical dashed line), ~ 5.5 min after the PSBL crossing at CL2. The PSBL crossing at CL1, which was further delayed (0052:10 UT: the second vertical dashed line), began ~ 7 min after that at CL2. The time lags among the spacecraft suggest that the thickening of plasma sheet evolved faster in the earthward direction than in the dawnward direction. One may be interested in some different local perturbations in the magnetic field between CL3 and CL4, which were rather close. For instance, before the PSBL crossings at both CL3 and CL4, large negative B_y changes were detected at CL3, but unclear at CL4. The different magnetic field signatures were seen also in B_x just after each PSBL crossing. In contrast, CL1, which was closer to CL2 in the X direction, observed B_y fluctuations similar to those at CL2, although some peaks were small. Especially, a large negative B_y excursion at CL1 just after the PSBL crossing was common to that at CL2.

[14] Next, eighth and ninth panels of Figure 8 respectively present the ion density and velocity (V_x : red, V_y : blue, V_z : green in GSM coordinates) measured by the Hot Ion Analyzer (HIA) instrument of the Cluster Ion Spectrometry (CIS) [*Rème et al.*, 2001]. The black curve in the ninth panel indicates the parallel component (V_{\parallel} , positive is earthward) to the local magnetic field. It should here be noted that during this event the HIA/CIS data were only available from CL1 because of operational reasons, and that the absolute value of the observed ion density was a little too small, but the relative variation was true (H. Rème, personal commu-

nication, 2011). In the ninth panel, we found that, there were no significant enhancements in the V_y and V_z components (less than 150 km s^{-1}) throughout the interval, whereas the transient V_x enhancements with $200\text{--}300 \text{ km s}^{-1}$ were observed for 0048–0050 UT and after 0052 UT. Each V_x enhancement at CL1 was accompanied by a small increase in ion density, a small decrease in $|B|$, and a small increase in B_z . For all of the V_x enhancements at CL1, we found that the magnitude of V_x was almost comparable to that of V_{\parallel} . This implies that the transient V_x enhancements at CL1 are associated with field-aligned high speed plasma flows in and near the PSBL (referred to as “ion beams” [e.g., *Takahashi and Hones*, 1988]), not with bursty bulk flows (BBFs) [e.g., *Angelopoulos et al.*, 1992; *Lyons et al.*, 1999] having a significant convective component perpendicular to the local magnetic field.

3. Discussion

3.1. Ionospheric Electrodynamics in Meso-Scale Auroral Undulations

[15] Here, let us first discuss the ionospheric electrodynamics in the vicinity of the meso-scale auroral arc undulations presented here, on the basis of the combined ground-based optical, magnetometer, and radar observations. We found many similarities in ground-based morphological features of the presented auroral arc undulations and the omega bands, although both have different spatial scales. It allows us to consider that the ionospheric current structures for our event are basically similar to those of omega bands studied by many authors [e.g., *Oppenorth et al.*, 1983; *Wild et al.*, 2000]. Eastward drifting omega bands are thought to be accompanied by a sequence of east-west oriented pairs of upward and downward FACs: the former flows from the bright area of omega bands, whereas the latter flows into the dark area. The pairs of upward and downward FACs drive pairs of vortical convections in the ionosphere, flowing in a clockwise (an anticlockwise) sense in the upward (downward) FAC region. The vortical convection flows (i.e., Hall current flows anti-parallel to the convection flows) propagating with omega bands result in magnetic Ps6 signatures on the ground. Figures 9a and 9b respectively show schematic pictures representing the auroral forms at 0044:00 UT and 0045:30 UT (see Figure 3), with the ionospheric plasma flows and FACs in the vicinity of them. Since both are viewed from space, the east-west direction of Figure 3 is reversed. Red and blue arrows show dominant directions of the LOS Doppler velocity observed with the Iceland East radar, whereas the black thick lines the ionospheric convection patterns inferred from the observed auroral structures and plasma flows. Similar to omega bands, we assume that upward (dotted red circle) and downward (crossed light-blue circle) FACs flow from the bright arc region and into the neighboring dark region, respectively. The upward (downward) FACs would be accompanied by a clockwise (counterclockwise) vortical plasma flow illustrated here. The positive and negative LOS velocities observed with the Iceland East radar might be regarded as a sign of the vortical plasma flows. In addition, the poleward plasma flow (i.e., equatorward Hall current flow) flowing between the paired vortices would give rise to a positive change in the east-west

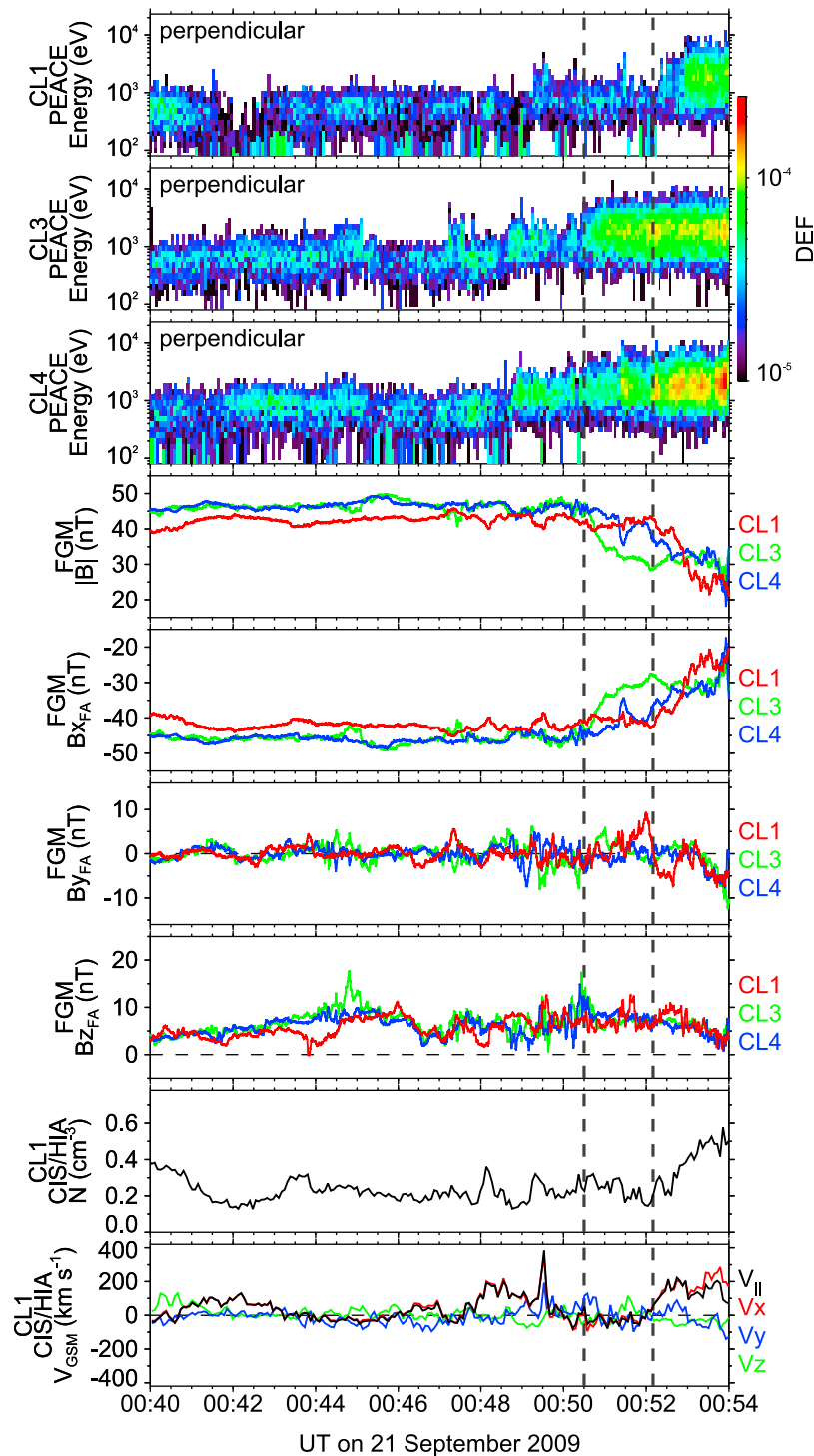


Figure 8. From first to seventh panels, energy-time spectrograms of electron DEF in directions perpendicular to the local magnetic field, magnetic field strength, and three components of the magnetic field in FA coordinates at CL1 (red), CL3 (green), and CL4 (blue) are presented for the interval of 0040–0054 UT. The PSBL crossing times are drawn by vertical dashed lines: 0050:30 UT for CL3 and CL4 and 0052:10 UT for CL1. Eighth and ninth panels respectively present the ion density and velocity (V_x : red, V_y : blue, V_z : green in GSM coordinates, V_{\parallel} : black) measured by the CIS/HIA at CL1.

component of the ground magnetic field. This is consistent with the periodic D component oscillation observed with ground magnetometer at TJO. As illustrated here, therefore, a possible interpretation for the nature of linkages between

the auroral forms, magnetic field variations, and plasma flows for our event is likely to be made in a manner that resembles the ionospheric structures of omega bands/Ps6.

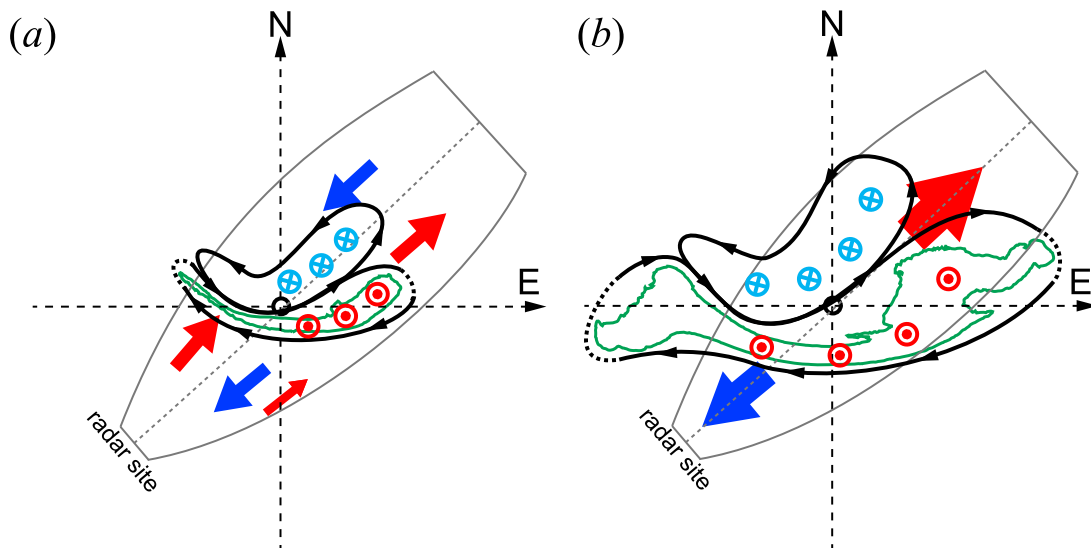


Figure 9. Schematic representations of the expected plasma flows and current systems in the vicinity of the auroral structures at (a) 0044:00 UT and (b) 0045:30 UT. Both are illustrated on the basis of the optical and radar observations shown in Figure 3, but view from space (i.e., the east-west direction is reversed). Each observed auroral structure is shown by green contour. Blue and red arrows indicate major directions of the LOS plasma flows observed in the radar FOV. Upward (dotted red circle) and downward (crossed light-blue circle) FACs, and vortical plasma flows (solid lines) are also shown. See text for details.

3.2. Model Field Line Mapping

[16] In general, there would be more or less some uncertainty for the magnetic field line mapping performed by the Tsyganenko magnetic field models because the modeled results are based on statistical studies. Nevertheless, any model is required to estimate the satellite footprint in the ionosphere. In order to test the magnetic field line mapping, we first attempted to compare the magnetic field data from CL2 with the outputs from a newer Tsyganenko model (TS04, for details see *Tsyganenko and Sitnov* [2005]), as well as from the T96 model used in this study. The accuracy of each model was evaluated by calculating the root mean square (RMS) error difference between the modeled outputs and measured data for the interval from 0040 UT to 0054 UT. Although the RMS results indicated that the T96 prediction was slightly better than the TS04 prediction, both model outputs approximately predicted the mean values of the measured magnetic field during this interval: from 28 nT to 30 nT in $|B|$, from -30 nT to -28 nT in B_x , from -3 nT to -2 nT in B_y , and from -5 nT to 3 nT in B_z . The model results did not always represent the dynamically changing magnetic field configuration at CL2, but they represented the average magnetic field topology, roughly resembling the actual field configuration with larger B_x and smaller B_z observed before 0045:05 UT. For the ionospheric footprints of CL2 predicted by the two models, moreover, the displacement between the two models was quite small, $\sim 0.5^\circ$ or less in latitude and $\sim 1^\circ$ or less in longitude.

[17] Second, let us consider how order the correspondence between the magnetotail region at CL2 and the ionospheric region at the CL2 footprint is plausible. The in situ field and particle measurements at CL2 before 0045:05 UT indicated that the CL2 location was in the southern lobe or at the lobe/PSBL interface of the highly stretched magnetotail

configuration. The ionospheric mapping from these magnetotail regions would be just outside the auroral poleward boundary or at the boundary. This is basically consistent with the predicted CL2 footprint (cf. Figure 4). After 0045:05 UT, the in situ measurements indicated that the magnetotail region at CL2 drastically changed from the PSBL into the PS. In that case, it is reasonable to suppose that the CL2 ionospheric footprint shifted equatorward, probably into the diffuse-like auroral region. However, effects of such rapid and localized changes at CL2 could not be always included in the model prediction. Indeed, the predicted CL2 footprint still remained near the auroral poleward boundary. We therefore concluded that the choice of model does not play a crucial role in the magnetic field line mapping, although there is slight difference between the T96 and TS04 outputs. Taking into account the in situ measurements at CL2 and the ionospheric counterpart at the footprint, a reasonable magnetic model field line mapping for this event is likely to be performed at least for the period before 0045:05 UT.

3.3. Near-Earth Tail FAC Signatures

[18] It is interesting to note that, whenever the bright and dark areas of the auroral arc undulations passed the CL2 footprint, CL2 observed large B_y fluctuations. In order to provide a better understanding of the in situ B_y fluctuations at CL2, a schematic picture of the auroral arc undulations and the related FAC structures is presented in Figure 10a. As shown in Figure 9, it is considered that the pairs of upward (bright area: dotted red circles) and downward (dark area: light-blue crossed circles) FACs successively propagated eastward across the CL2 footprint in the ionosphere with the drifting auroral arc undulations. The FAC signatures would also be detected at the CL2 location that changed from the southern lobe to PSBL and then to CPS. The magnetotail

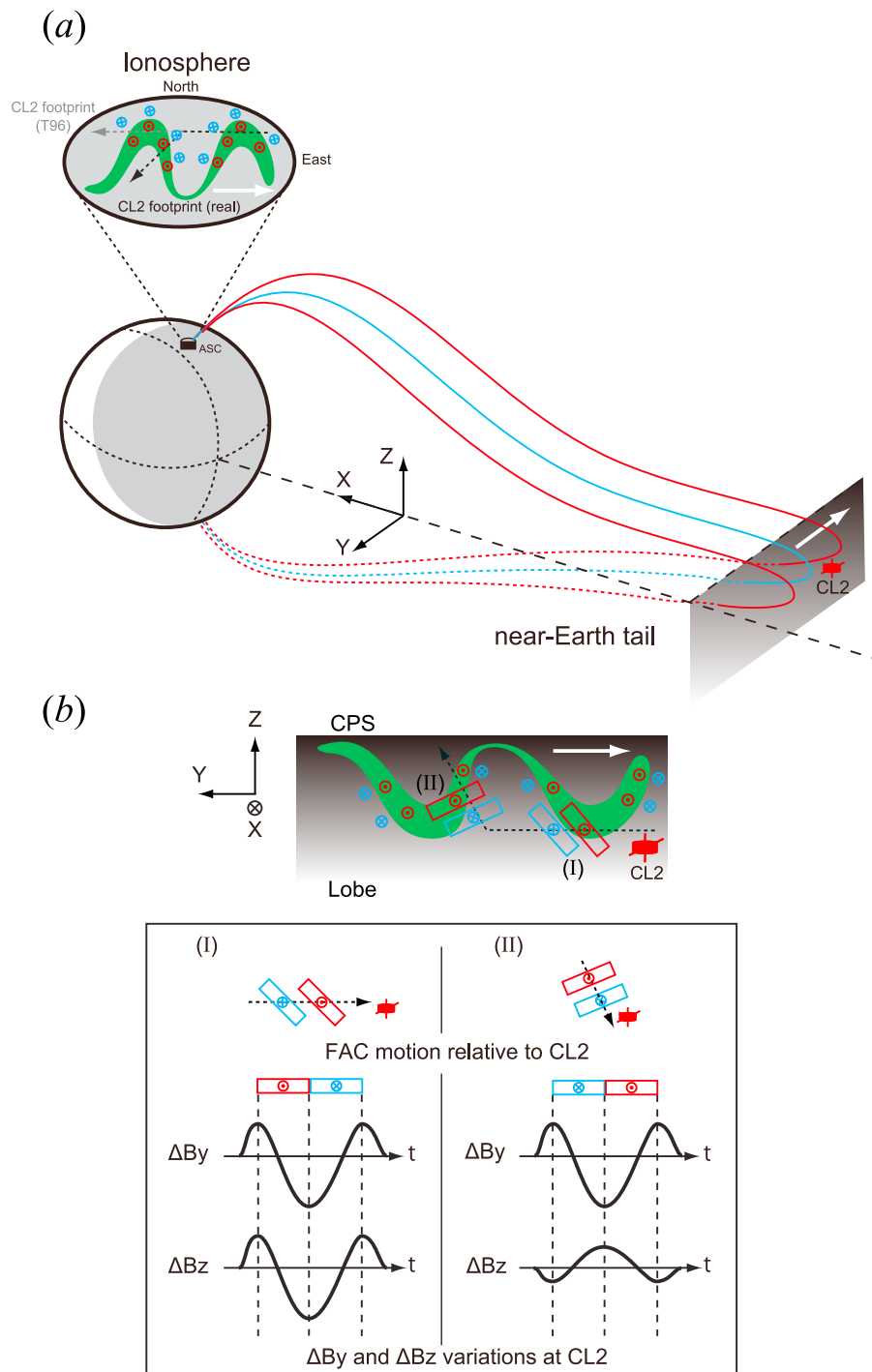


Figure 10. (a and b) Schematic diagrams illustrating a possible relationship between the in situ magnetic field variation at CL2 in the central near tail region and the optical auroral variation at its ionospheric footprint for this event. See text for details.

mapping of the observed auroral structures using the T96 model suggests that the lobe-plasma sheet boundary had local undulations. Figure 10b schematically represents the FAC distribution in the Y-Z cross section of the CL2 location, together with the local B_y and B_z variations at CL2 caused by the FAC crossings. In this scenario, we assume that the FAC has a finite sheet-like structure and flows in the PSBL. Before 0045:05 UT (corresponding to (I) of

Figure 10b), CL2 adjacent to PSBL would detect modulations of the magnetic field produced by the Y directional (eastward) motion of the FACs tilted slightly due to the undulating boundary structure. In the case that first the upward (i.e., tailward) FAC and then the downward (i.e., earthward) FAC crosses over CL2, the FAC signatures at CL2 would be characterized by the B_y and B_z changes, consisting of small positive gradient just before the upward

FAC crossing, larger negative gradient in the upward FAC region, larger positive gradient in the downward FAC region, and small negative gradient after the downward FAC crossing (see Figure 10b). According to the CL2 observations after 0045:05 UT, on the other hand, the PSBL and CPS regions were approaching to CL2, probably with the aid of the plasma sheet thickening. As a result, CL2 crossed over PSBL in the Z direction and then entered into CPS (corresponding to (II) of Figure 10b). In that case, CL2 would detect signatures of the FACs with the Z directional motion as well as the Y directional motion. Assuming that CL2 crosses the eastward drifting FACs in the Z direction, CL2 would first detect downward FAC signature on the lobe-side boundary of PSBL and then upward FAC signature on the CPS-side boundary. The FAC polarities are the same as those of the midnight poleward boundary current system, previously reported by *Fukunishi et al.* [1993]. They demonstrated that the poleward boundary current system in the ionosphere is composed of a pair of a downward FAC on the poleward side and an upward FAC on the equatorward side and that its current system is mapped to the PSBL region. The FAC signature at CL2 would be detected as mainly a negative excursion in the B_y field (i.e., $dB_y/dt < 0$ in the downward FAC region and $dB_y/dt > 0$ in the upward FAC region) with some B_z variations.

[19] In order to verify our hypothesis mentioned above, we now turn to the comparison between both data in Figure 7. Before 0045:05 UT, a train of remarkable local maximum (A: upward FAC), minimum (B: downward FAC), and maximum (C: upward FAC) in the auroral luminosity was observed at the CL2 footprint. Each local maximum (minimum) in the auroral luminosity would be related to upward (downward) FAC. During the same interval, CL2 successively detected positive and negative changes in the B_y and B_z field. Just for reference, approximate local FAC signatures at CL2 deduced from our hypothesis are color-coded (red: upward FAC, blue: downward FAC) in the third and fourth panels of Figure 7. The observed B_y and B_z signatures in each color-coded area are fairly similar to those deduced from an eastward passage of FACs, as drawn schematically in the left panel of Figure 10b. Therefore, at least during this interval for which the brighter auroral arc undulations passed eastward across near the CL2 footprint, a series of the upward-downward-upward FAC polarities deduced from the auroral luminosity at the CL2 footprint appears to roughly coincide with that deduced from the in situ magnetic field fluctuations at CL2. Note that most of the B_y and B_z field variations at CL2 slightly preceded the auroral luminosity variation at the CL2 footprint. This may be attributed to a propagation time of Alfvén waves from the CL2 location to the ionosphere. However, it should also be noted that before ~0043 UT there was not always clear correspondence between the in situ field and auroral luminosity variations: large changes in the in situ B_y and B_z field were observed at CL2, whereas there were no significant luminosity variations at the CL2 footprint. This might be due to ambiguity in the accuracy of the field line mapping, because the CL2 location was more or less changing in the tail region.

[20] Just after 0045:05 UT (i.e., during the PSBL crossing at CL2), on the other hand, a marked negative B_y excursion with amplitude of 10 nT or more was observed at CL2 with a

small positive B_z excursion. If our hypothesis were correct, the observed B_y and B_z signatures were in reasonable agreement with the deduced signatures, as drawn schematically in the right panel of Figure 10b. Then, the large negative B_y excursion would be produced by a pair of downward and upward FACs, appearing when the PSBL region expanding in the Z direction crosses over CL2. The in situ downward FAC signature (i.e., negative B_y gradient) during the PSBL crossing at CL2 may correspond to the early period of local minimum (D: downward FAC) in the auroral luminosity at the CL2 footprint. For most of the PSBL crossing interval at CL2, however, clear one-to-one correspondence between FAC signatures deduced from the in situ field and the auroral luminosity were poor or not found. As discussed in section 3.2, the discrepancy between the in situ and ionospheric observations might be attributed to uncertainty in the T96 ionospheric mapping after 0045:05 UT. That is, after 0045:05 UT the “real” CL2 footprint in the ionosphere is considered to shift equatorward across the auroral undulation structure at the poleward boundary (as shown by black dashed arrow in Figure 10a), whereas the predicted CL2 footprint remains near the auroral poleward boundary (as shown by gray dotted arrow in Figure 10a).

3.4. Eastward Propagation of FACs

[21] A series of the meso-scale auroral arc undulations was found to drift eastward at a speed of 0.9–2.2 km s⁻¹ in the ionosphere, comparable to the average speed of the classical omega-bands. This drift speed corresponded to ~40 km s⁻¹ in the near-Earth tail region of the CL2 location, as deduced from the magnetotail projections given by the T96 model (Figure 5). During this event, both CL3 and CL4 did not observe B_y fluctuations similar to those at CL2, although the PSBL crossing was detected. In contrast, CL1, which was located at ~2.0 R_E (12,740 km) dawnward of CL2 in the Y direction, observed B_y fluctuations similar to those at CL2 about 7 min late (Figure 8). The differences among the spacecraft imply that the FACs flow in a boundary region tailward of CL3/CL4 (–12 R_E). If the in situ B_y fluctuations at CL1 and CL2 were produced by the exact same FACs, a time lag between them might be due to the dawnward propagation of the localized FACs. The dawnward propagation speed of the FAC signatures estimated from the Y directional separation (12,740 km) and time lag (425 s) between CL1 and CL2 is ~30 km s⁻¹, in roughly agreement with that inferred from the auroral undulation structures projected onto the CL2 location. However, the B_y fluctuation at CL1 did not always correspond to the auroral luminosity variation at the CL1 footprint (not shown here). This might be because the CL1 footprint was mapped near the eastward edge of the ASC field-of-view.

3.5. Poynting Flux and FAC Intensity

[22] Poynting flux is one of key parameters to understand electromagnetic energy transport in the magnetosphere-ionosphere coupling system. Using Polar observations at geocentric distances of 4–7 R_E, some previous studies demonstrated that large amplitude electric fields associated with Alfvén waves are often observed during the PSBL crossings [e.g., *Wygant et al.*, 2000; *Keiling et al.*, 2001]. Such large amplitude electric fields are accompanied by Poynting flux toward the ionosphere sufficient to power

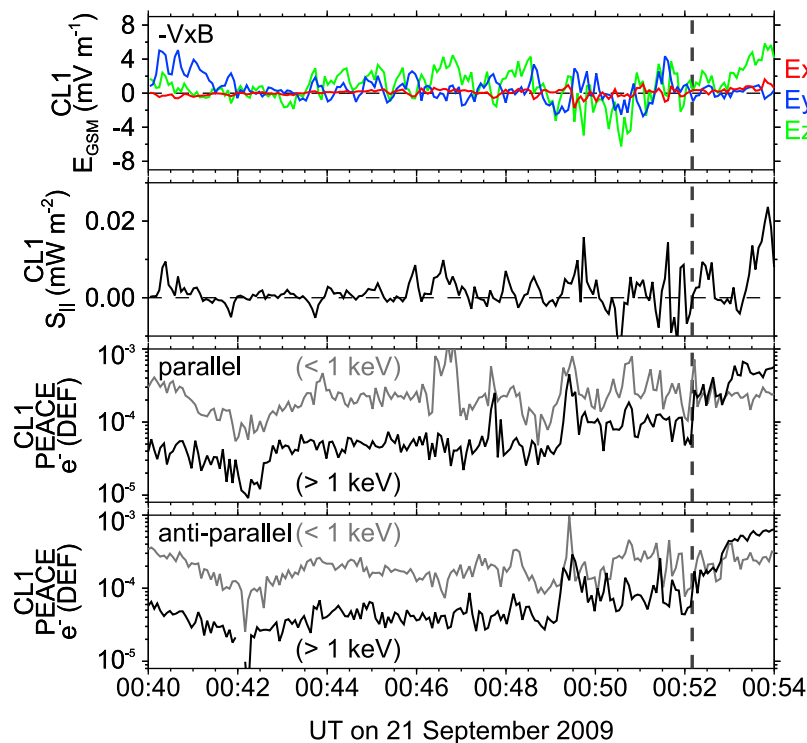


Figure 11. From top to bottom, the electric field (E_x : red, E_y : blue, E_z : green) in GSM coordinates calculated from $\mathbf{E} = -\mathbf{V} \times \mathbf{B}$ (where, \mathbf{E} : electric field, \mathbf{V} : ion velocity, \mathbf{B} : magnetic field), field-aligned component of Poynting flux (S_{\parallel} , positive is earthward), and parallel (tailward) and anti-parallel (earthward) components of the integrated electron DEFs, obtained by CL1 between 0040 UT and 0054 UT on September 21, 2009. In the bottom two panels, the black and gray curves indicate the integrated DEFs of high-energy (>1 keV) and low-energy (<1 keV) electrons, respectively. Vertical dashed line indicates the PSBL crossing time (0052:10 UT) at CL1.

intense aurora in the ionosphere [Keiling *et al.*, 2002]. Here, in order to confirm whether Poynting flux at the Cluster location is sufficient to drive the auroral arc undulations in the ionosphere, let us attempt an order estimate.

[23] For the estimation of field-aligned Poynting flux, both 3-dimensional (3-D) vectors of electric and magnetic fields are required. In this study, three components of the electric field were calculated from $\mathbf{E} = -\mathbf{V} \times \mathbf{B}$ (where, \mathbf{E} : electric field, \mathbf{V} : ion velocity, \mathbf{B} : magnetic field), using the 3-D ion velocity data measured by the CIS instrument and the magnetic field measured by the FGM instrument. Since the CIS data were only available from CL1, the magnitude of Poynting flux at CL2 was indirectly deduced from Poynting flux at CL1, by assuming that the eastward drifting FAC signatures at CL2 also passed over CL1 with the same structure. In top two panels of Figure 11, three components of the calculated electric field (E_x : red, E_y : blue, E_z : green) in GSM coordinates and field-aligned component of Poynting flux (S_{\parallel} , positive is earthward) are presented. Note here that since the calculated electric field and Poynting flux are on a time scale longer than the satellite spin period (~ 4 s), their rapid, shorter period variations are filtered out. As reference, the parallel (tailward) and anti-parallel (earthward) components of the integrated DEFs of low-energy (less than 1 keV, gray curve) and high-energy (more than 1 keV, black curve) electrons are presented in the bottom two panels of Figure 11. The field-aligned Poynting flux was

calculated from the perturbation electric and magnetic fields. The vertical dashed line indicates the PSBL crossing time (0052:10 UT) at CL1 shown in Figure 8. Before 0049 UT, Poynting flux had no significant variations (less than 0.01 mW/m²), but it was obviously enhanced after 0049 UT, i.e., during the interval in which the eastward drifting FACs would pass over CL1. The peak value of the enhanced Poynting flux at CL1 exceeded 0.01 mW/m², which was no more than the half of Poynting flux in the plasma sheet $\sim 8 R_E$ tailward of the Earth [Wild *et al.*, 2011]. Just during the Poynting flux enhancements, the parallel and anti-parallel electron DEFs were also slightly enhanced. At least a part of the Poynting flux enhancements appeared to be coincident with the electron DEF enhancements. If Poynting flux with 0.01 mW/m² at the Cluster location is mapped to ionospheric altitudes [see Keiling *et al.*, 2002, equation (3)], the mapped Poynting flux is 13 mW/m². According to the Polar observations by Keiling *et al.* [2002], such a mapped Poynting flux might be sufficient to power discrete aurora, like the auroral arc undulations presented here.

[24] For this event, the intensity of the eastward drifting upward/downward (tailward/earthward) FAC sheets can also roughly be estimated from the magnetic field variations at a single satellite by assuming that the satellite keeps stationary during the eastward passage of FACs. The FAC intensity estimated from the CL2 magnetic field deviations was of the order of 8 – 20 mA m⁻¹ for the interval from 0043:00 to

0045:10 UT and $\sim 12 \text{ mA m}^{-1}$ just after 0045:10 UT. The FAC intensity during the PSBL crossing at CL2 was approximately consistent with that ($8\text{--}12 \text{ mA m}^{-1}$) at CL1. Our order-of-magnitude estimates of the FAC intensity are comparable to the previous in situ measurements ($6\text{--}30 \text{ mA m}^{-1}$) at the magnetotail PSBL at distances between $10 R_E$ and $20 R_E$ [Aubry et al., 1972; Frank et al., 1981]. When mapped into ionospheric altitudes [cf. Aubry et al., 1972], the mapped FAC sheet intensities are of the order of $0.25\text{--}0.62 \text{ A m}^{-1}$, which are in reasonable agreement with those measured at low altitudes in the auroral region [e.g., Iijima and Potemra, 1978].

4. Summary

[25] We have presented here the combined ground-based measurements of an eastward drifting meso-scale auroral arc undulation event, together with the in situ measurements at Cluster spacecraft located in the central near-Earth tail ($11\text{--}14 R_E$ down tail). In particular, the ionospheric footprint of CL2 was close to the auroral forms drifting along the auroral poleward boundary. The combined ground-based optical, magnetometer, and radar data have indicated that our event and the classical omega-bands/Ps6 had a lot in common, in terms of the auroral features as well as the behavior of ionospheric plasma flows and current systems within them, except for spatial scale. The ionospheric spatial and temporal structures imply the presence of the paired upward and downward FACs, which also propagate eastward with the auroral motion. On the other hand, the magnetospheric counterpart of the auroral undulations was identified as strong perturbations in the in situ B_y and/or B_z field. It is found that the B_y and/or B_z field perturbations at CL2 was observed when the bright (upward FAC) and dark (downward FAC) regions of the drifting auroral arc undulations passed across the CL2 footprint. Thus, the in situ magnetic field changes at CL2 could be considered as a manifestation of pairs of FACs, being a possible main driver of the meso-scale auroral arc undulations and related ionospheric flow/current signatures. Similar in situ magnetic field changes were observed also at CL1 which was $\sim 2 R_E$ dawnward away from CL2, but they were delayed in comparison with CL2. The time delay would be a result of the longitudinal propagation delay of FACs from CL2 to CL1, which is in reasonable agreement with the eastward motion of auroral undulations in the ionosphere. The simultaneous ground-satellite observations reported here provides a direct magnetosphere-ionosphere linkage for the spatial and temporal evolution of the meso-scale arc undulations at the auroral poleward boundary, probably due to FACs propagating eastward in and near the PSBL. However, our observations cannot provide definite answer to the question where and how the FACs are generated in the near-Earth tail, which will be the subject of future work.

[26] **Acknowledgments.** The authors acknowledge S. C. Buchert for providing the Cluster high-resolution FGM data, M. Goldstein for providing the Cluster PEACE data, and H. Rème for providing the Cluster CIS data. This work is partially supported by a Grant-in-Aid for Scientific Research B (21403007) and the Inter-university Upper atmosphere Global Observation NETwork (IUGONET) project funded by the Ministry of Education, Culture, Sports, Science and Technology of Japan. The production of this paper was supported by an NIPR publication subsidy. S. E. M. and M. L. were funded by STFC grant ST/H002480/1.

[27] Robert Lysak thanks the reviewers for their assistance in evaluating this paper.

References

- Akasofu, S.-I. (1974), A study of auroral displays photographed from DMSP-2 satellite and from the Alaska meridian chain of stations, *Space Sci. Rev.*, *16*, 617–725, doi:10.1007/BF00182598.
- Akasofu, S.-I., and D. S. Kimball (1964), The dynamics of the aurora—1. Instabilities of the aurora, *J. Atmos. Terr. Phys.*, *26*, 205–211, doi:10.1016/0021-9169(64)90147-3.
- Angelopoulos, V., W. Baumjohann, C. F. Kennel, F. V. Coroniti, M. G. Kivelson, R. Pellat, R. J. Walker, H. Lühr, and G. Paschmann (1992), Bursty bulk flows in the inner central plasma sheet, *J. Geophys. Res.*, *97*(A4), 4027–4039, doi:10.1029/91JA02701.
- Aubry, M. P., M. G. Kivelson, R. L. McPherron, C. T. Russell, and D. S. Colburn (1972), Outer magnetosphere near midnight at quiet and disturbed times, *J. Geophys. Res.*, *77*(28), 5487–5502, doi:10.1029/JA077i028p05487.
- Baker, K. B., and S. Wing (1989), A new magnetic coordinate system for conjugate studies at high latitudes, *J. Geophys. Res.*, *94*(A7), 9139–9143, doi:10.1029/JA094iA07p09139.
- Balogh, A., et al. (2001), The Cluster magnetic field investigation: Overview of in-flight performance and initial results, *Ann. Geophys.*, *19*, 1207–1217, doi:10.5194/angeo-19-1207-2001.
- Chisham, G., et al. (2007), A decade of the Super Dual Auroral Radar Network (SuperDARN): Scientific achievements, new techniques and future directions, *Surv. Geophys.*, *28*, 33–109, doi:10.1007/s10712-007-9017-8.
- Frank, L. A., R. L. McPherron, R. J. DeCoster, B. G. Burek, K. L. Ackerson, and C. T. Russell (1981), Field-aligned currents in the Earth's magnetotail, *J. Geophys. Res.*, *86*(A2), 687–700, doi:10.1029/JA086iA02p00687.
- Fukunishi, H., Y. Takahashi, T. Nagatsuma, T. Mukai, and S. Machida (1993), Latitudinal structures of nightside field-aligned currents and their relationships to the plasma sheet regions, *J. Geophys. Res.*, *98*(A7), 11,235–11,255, doi:10.1029/92JA02031.
- Hosokawa, K., T. Motoba, A. S. Yukimatu, S. E. Milan, M. Lester, A. Kadokura, N. Sato, and G. Björnsson (2010), Plasma irregularities adjacent to auroral patches in the postmidnight sector, *J. Geophys. Res.*, *115*, A09303, doi:10.1029/2010JA015319.
- Iijima, T., and T. A. Potemra (1978), Large-scale characteristics of field-aligned currents associated with substorms, *J. Geophys. Res.*, *83*(A2), 599–615, doi:10.1029/JA083iA02p00599.
- Janhunen, P., and A. Huuskonen (1993), A numerical ionosphere-magnetosphere coupling model with variable conductivities, *J. Geophys. Res.*, *98*(A6), 9519–9530, doi:10.1029/92JA02973.
- Johnstone, A. D., et al. (1997), A plasma electron and current experiment, *Space Sci. Rev.*, *79*, 351–398, doi:10.1023/A:1004938001388.
- Jorgensen, A. M., H. E. Spence, T. J. Hughes, and D. McDiarmid (1999), A study of omega bands and Ps6 pulsations on the ground, at low altitude and at geostationary orbit, *J. Geophys. Res.*, *104*(A7), 14,705–14,715, doi:10.1029/1998JA900100.
- Keiling, A., J. R. Wygant, C. Cattell, M. Johnson, M. Temerin, F. S. Mozer, C. A. Kletzing, J. Scudder, and C. T. Russell (2001), Properties of large electric fields in the plasma sheet at $4\text{--}7 R_E$ measured with Polar, *J. Geophys. Res.*, *106*(A4), 5779–5798, doi:10.1029/2000JA900130.
- Keiling, A., J. R. Wygant, C. Cattell, W. Peria, G. Parks, M. Temerin, F. S. Mozer, C. T. Russell, and C. A. Kletzing (2002), Correlation of Alfvén wave Poynting flux in the plasma sheet at $4\text{--}7 R_E$ with ionospheric electron energy flux, *J. Geophys. Res.*, *107*(A7), 1132, doi:10.1029/2001JA900140.
- Lyons, L. R., T. Nagai, G. T. Blanchard, J. S. Samson, T. Yamamoto, T. Mukai, A. Nishida, and S. Kokubun (1999), Association between Geotail plasma flows and auroral poleward boundary intensifications observed by CANOPUS photometers, *J. Geophys. Res.*, *104*(A3), 4485–4500, doi:10.1029/1998JA900140.
- Milan, S. E., N. Sato, M. Lester, T. K. Yeoman, Y. Murata, H. Doi, and T. Saemundsson (2002), The spectral characteristics of E region radar echoes co-located with and adjacent to visual auroral arcs, *Ann. Geophys.*, *20*, 795–805, doi:10.5194/angeo-20-795-2002.
- Motoba, T., K. Hosokawa, N. Sato, A. Kadokura, and G. Björnsson (2010), Varying interplanetary magnetic field By effects on interhemispheric conjugate auroral features during a weak substorm, *J. Geophys. Res.*, *115*, A09210, doi:10.1029/2010JA015369.
- Motoba, T., K. Hosokawa, Y. Ogawa, N. Sato, A. Kadokura, S. C. Buchert, and H. Rème (2011), In situ evidence for interplanetary magnetic field induced tail twisting associated with relative displacement of conjugate auroral features, *J. Geophys. Res.*, *116*, A04209, doi:10.1029/2010JA016206.
- Ohtani, S., S. Kokubun, R. C. Elphic, and C. T. Russell (1988), Field-aligned current signatures in the near-tail region: 1. ISEE observations

- in the plasma sheet boundary layer, *J. Geophys. Res.*, *93*(A9), 9709–9720, doi:10.1029/JA093iA09p09709.
- Opgenoorth, H. J., J. Oksman, K. U. Kaila, E. Nielsen, and W. Baumjohann (1983), Characteristics of eastward drifting omega bands in the morning sector of the auroral oval, *J. Geophys. Res.*, *88*(A11), 9171–9185, doi:10.1029/JA088iA11p09171.
- Rees, M. H. (1963), Auroral ionization and excitation by incident energetic electrons, *Planet. Space Sci.*, *11*, 1209–1218, doi:10.1016/0032-0633(63)90252-6.
- Rème, H., et al. (2001), First multispacecraft ion measurements in and near the Earth's magnetosphere with identical Cluster ion spectrometry (CIS) experiment, *Ann. Geophys.*, *19*, 1303–1354, doi:10.5194/angeo-19-1303-2001.
- Saito, T. (1978), Long-period irregular magnetic pulsations, Pi3, *Space Sci. Rev.*, *21*, 427–467, doi:10.1007/BF00173068.
- Takahashi, K., and E. W. Hones Jr. (1988), ISEE 1 and 2 observations of ion distributions at the plasma sheet-tail lobe boundary, *J. Geophys. Res.*, *93*(A8), 8558–8582, doi:10.1029/JA093iA08p08558.
- Tsyganenko, N. A. (1995), Modeling the Earth's magnetospheric magnetic field confined within a realistic magnetopause, *J. Geophys. Res.*, *100*(A4), 5599–5612, doi:10.1029/94JA03193.
- Tsyganenko, N. A., and M. I. Sitnov (2005), Modeling the dynamics of the inner magnetosphere during strong geomagnetic storms, *J. Geophys. Res.*, *110*, A03208, doi:10.1029/2004JA010798.
- Wild, J. A., T. K. Yeoman, P. Eglitis, and H. J. Opgenoorth (2000), Multi-instrument observations of the electric and magnetic field structure of omega bands, *Ann. Geophys.*, *18*, 99–110, doi:10.1007/s00585-000-0099-6.
- Wild, J. A., et al. (2011), Midnight sector observations of auroral omega bands, *J. Geophys. Res.*, *116*, A00I30, doi:10.1029/2010JA015874.
- Wygant, J. R., et al. (2000), Polar spacecraft based comparisons of intense electric fields and Poynting flux near and within the plasma sheet tail lobe boundary to UVI images: An energy source for the aurora, *J. Geophys. Res.*, *105*(A8), 18,675–18,692, doi:10.1029/1999JA900500.
- Yamamoto, T., S. Inoue, and C.-I. Meng (1997), Formation of auroral omega bands in the paired region 1 and region 2 field-aligned current system, *J. Geophys. Res.*, *102*(A2), 2531–2544, doi:10.1029/96JA02456.